Bending performance and failure behavior of 3D printed continuous fiber reinforced composite corrugated sandwich structures with shape memory capability

Chengjun Zeng [a], Liwu Liu [a], Wenfeng Bian [b],*, Jinsong Leng [c], Yanju Liu [a],*

[a] Department of Astronautical Science and Mechanics, Harbin Institute of Technology (HIT), P.O. Box 301, No. 92 West Dazhi Street, Harbin 150001, People's Republic of China
[b] Department of Civil Engineering, Harbin Institute of Technology (HIT), Weihai 264209, People's Republic of China
[c] Center for Composite Materials and Structures, Harbin Institute of Technology (HIT), P.O. Box 3011, No. 2 YiKuang Street, Harbin 150080, People's Republic of China

ARTICLE INFO

ABSTRACT

Here, a co-extrusion-based 3D printing technology was applied to integrally manufacture continuous fiber reinforced composite trapezoidal corrugated sandwich structures (CFRCTCSs) with shape memory capability. The theoretical models were developed to analyze the bending performance and failure behavior of the 3D printed CFRCTCSs with various geometric configurations and verified by three-point bending tests. Good agreement between the predictions and the experimental measurements was achieved. Considering four dominant failure modes including face yielding, face buckling, core shear failure and indentation collapse, the failure maps based on the analysis models were constructed to highlight the failure mechanism of CFRCTCSs and provide a practical guide for the design of lightweight sandwich structures. Shape recovery tests were performed to confirm the shape memory capability of the 3D printed CFRCTCSs. Finally, the comparison of the bending properties with several competing structures indicates that the 3D printed CFRCTCSs possess the potential to provide new opportunities for lightweight systems and multifunctional applications.

1. Introduction

Sandwich structures are a type of laminated composites that have been available due to their high stiffness-to-weight and lightweight features [1,2]. The most common sandwich structure consists of two thin skins and an inner core made of honeycomb or polymer foam with low density and low modulus [3]. The high thickness of the core provides a higher moment of inertia and improves the bending stiffness of the sandwich panel [4]. In another type of sandwich structure, the core is corrugated, which can be designed in various geometric shapes, such as triangular, trapezoidal, sinusoidal and hexagonal cellular shapes [5,6]. These corrugated sandwich structures can provide superior shock absorption capacity and bending resistance, which makes them a promising candidate in aeronautics, aerospace and marine engineering as an integrated protection system [7]. Some theoretical, experimental and numerical investigations on the bending properties of metallic corrugated sandwich structures have been published. Seong et al. [8] theoretically and experimentally investigated the quasi-isotropic bending behavior of metal corrugated sandwich panels. Valdevit et al. [9] studied the transverse and longitudinal bending

properties of corrugated sandwich steel plates through experimental measurements and numerical calculations.

When both the panels and the corrugated core are made of fiber reinforced composites (FRCs), the corrugated sandwich structure may be more attractive for structural applications. Because FRC corrugated sandwich structures not only further reduce the weight compared to metal corrugated sandwich structures, but also the tunable mechanical properties of the composites provide even greater design flexibility for corrugated sandwich structures [10,11]. However, the traditional manufacturing processes of such composite corrugated sandwich structures such as hot press molding, filament winding, pultrusion and vacuum-assisted molding require autoclaves or complex rigid molds for non-autoclave processes, thus hindering the wide application of composite corrugated sandwich structures [12].

The advances in rapid prototyping technologies such as additive manufacturing, also commonly referred to as 3D printing, offer the possibility to easily fabricate cellular cores with free-form 2D and 3D topologies, which are quite difficult to be fabricated with general manufacturing processes, e.g. hot pressing and injection molding [13]. The most widely used 3D printing methods are extrusion-based methods

and powder bed fusion-based methods, such as fused filament fabrication (FFF) [14,15], direct ink writing (DIW) [16] and selective laser sintering (SLS) [17]. These methods form 3D objects by depositing raw materials line-by-line and then layer-by-layer [18]. Related research demonstrates that new sandwich structures integratedly constructed by 3D printing, especially those with topology optimized microarchitecture, usually exhibit high bonding strength between the panels and the core, which contributes to excellent bending properties [19]. When the raw materials are programmable materials such as shape memory polymers (SMPs) [20,21], 3D printed objects often possess the ability to transform their physical characteristics through predetermined stimuli [22]. The manufacturing process combining programmable materials and 3D printing technology brings new opportunities for the design and fabrication of multifunctional lightweight structures.

Recently, continuous fiber reinforced thermoplastic polymer composites have been successfully manufactured through an innovative 3D printing process [23–26]. This process can also be used to construct continuous fiber reinforced composite lightweight structures (CFRCLSs) with controlled properties, which shows a broad prospect for low-cost manufacturing of FRC parts and multifunctional structures [27]. Hou et al. [28] proposed the cross lap and panel-core lap design strategies to fabricate CFRCLSs with complex configurations through 3D printing, and initially investigated the compression properties of CFRCLSs. Sugiyama et al. [29] used continuous carbon fiber and fiber tension to fabricate sandwich structures with various core shapes as a single piece. Essassi et al. [30] studied the bending fatigue behavior of 3D printed bio-based composite sandwich beams. However, although some preliminary investigations on 3D printing and mechanical behavior of CFRCLSs mentioned above have been reported, there is still a lack of extensive theoretical and experimental research on the bending

performance and failure behavior of the 3D printed CFRCLSs. Moreover, there is almost no precedent of using SMPs for the 3D printed CFRCLSs.

In the present study, the bending performance and failure mechanism of the integrated continuous fiber reinforced composite trapezoidal corrugated sandwich structures (CFRCTCSs) fabricated by combining SMPs and co-extrusion-based FFF 3D printing process were investigated. The analysis models were proposed to predict the bending properties and failure modes of the 3D printed CFRCTCSs with various geometric configurations. Corresponding three-point bending experiments were carried out to validate the analysis models, and the failure maps based on different collapse mechanisms of the sandwich structures were constructed. Moreover, the shape recovery tests were performed to evaluate the shape memory capability of the 3D printed CFRCTCSs. Finally, the bending properties of the 3D printed CFRCTCSs were compared with several competitive sandwich structures to gauge their overall potential.

2. Experimental methods

2.1. Design of the sandwich structures

The corrugated plates are continuous periodic structures composed of the same elements. The geometry of the element can severely affect the mechanical properties of these corrugated plates. To describe a periodic trapezoidal element, as shown in Fig. 1a, a series of geometric parameters are defined as: the thickness t of the core wall, the panel thickness t_f, the length l of the horizontal core wall, the height h of the single-layer corrugated core and the corrugation angle ψ. The trapezoidal corrugated sandwich panel consists of a single or multi-layer periodic corrugated core and the upper and lower thin skins.
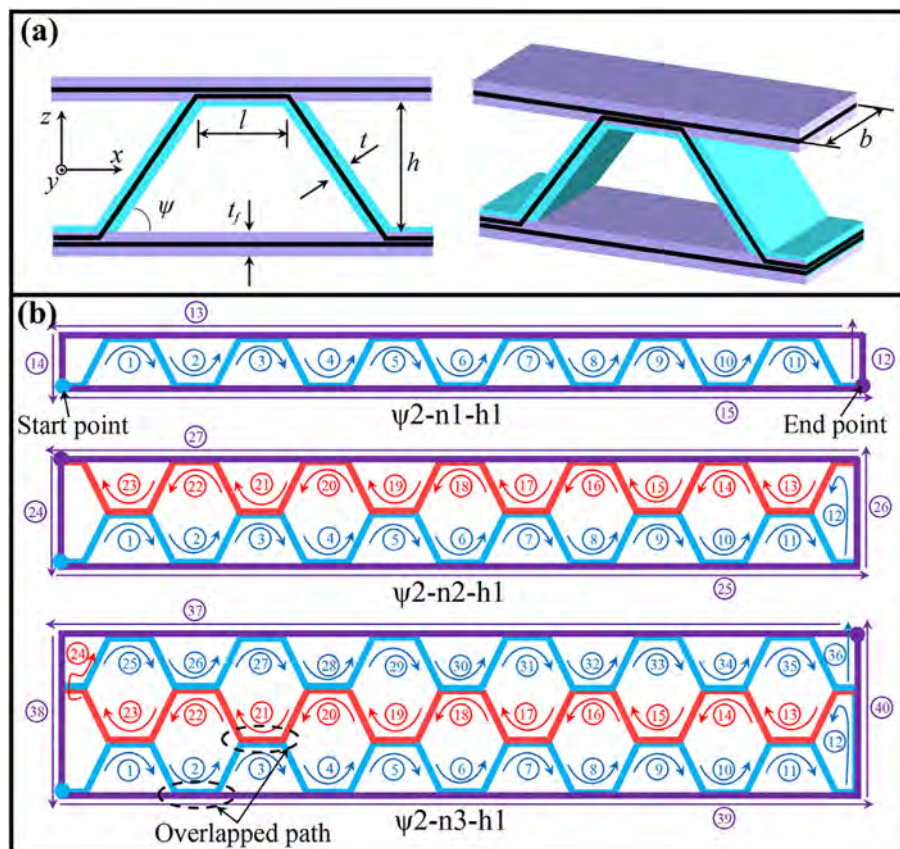

Fig. 1. Schematic diagram of (a) element and (b) printing path design of the trapezoidal corrugated sandwich panel.

According to the geometric relationship between the element and the sandwich structure, the relative density of the multi-layer trapezoidal corrugated sandwich structures can be expressed as:

$$\bar{\rho}_s = \frac{\rho_s}{\rho_r} = \frac{nt(l\sin\psi + h) + 2t_f(l\sin\psi + h\cos\psi)}{(h_c + 2t_f)(l\sin\psi + h\cos\psi)} \tag{1}$$

where, ρ_s and ρ_r denote the density of the multi-layer corrugated sandwich structures and the material, respectively, $h_c = nh + t$ is the total height of the multi-layer corrugated core, and n represents the number of layers of the corrugated core in the sandwich structure.

In this work, the density of the 3D printed continuous fiber reinforced composites was $\rho_r = 1390$ kg/m^3. Some geometric parameters were fixed as $t = 2.3$ mm, $t_f = 2.3$ mm, $b = 35$ mm, while other geometric parameters such as the corrugation angle ψ, the number of layers n and the height h of the single-layer corrugated core were considered as design variables. The 3D printed CFRCTCSs were grouped according to design variables including the corrugation angle ψ (ie, 52° "$\psi1$", 63° "$\psi2$" and 90° "$\psi3$"), the number of core layers n (ie, one layer "n1", double layers "n2" and three layers "n3"), and the single-layer core height h (ie, 9 mm "h1", 15 mm "h2" and 21 mm "h3"). For example, $\psi2$-n2-h1 represents a specimen with the corrugation angle ψ of 63°, the number of layers n of 2 and the single-layer core height h of 9 mm.

2.2. Manufacturing process

An FFF 3D printer with two feeding channels as shown in Fig. 2a was used to fabricate complex components made of continuous fiber reinforced polymer composites. The original single-material printer before modification was produced by Shenzhen Creality 3D Technology Co., Ltd., China. As shown in Fig. 2b, continuous fiber and flexible material are respectively introduced into the extruder from the corresponding feeding channels. The heating device in the extruder provides sufficient heat to melt the flexible thermoplastic material from a solid-state to a molten state. Then, under the action of traction, the fiber bundle impregnated with the molten material is pulled out of the nozzle and solidified on the platform. The printing path schemes of typical CFRCTCSs including $\psi2$-n1-h1, $\psi2$-n2-h1 and $\psi2$-n3-h1 are listed in Fig. 1b. Herein, the single-layer printing path starts from the "start point" and ends with the "end point" according to the serial number, and there is no nozzle jumping in the process. After completing the single-layer printing, the extruder turns backwards again from "end point" to "start point" to complete the printing of the next layer. In order to enhance the adhesion between the adjacent core walls as well as the corrugated core and the panels, the path overlapping is considered in the path design, as shown by the dotted elliptical frame marked in Fig. 1b. The overlapping percentage of two adjacent paths is approximately 80%.

In this study, the flexible material used to fabricate CFRCTCSs was the semi-crystalline shape memory polylactic acid (PLA) prepared by the research group of Professor Jinsong Leng at Harbin Institute of Technology [15,31]. The melting temperature of the PLA filaments was about 170 °C. The continuous carbon fiber bundle was T300B-3000-40B produced by Toray Co., Ltd. of Japan. The printing parameters were set to a layer thickness of 0.4 mm, a nozzle diameter of 2 mm, a printing speed of 100 mm/min and a nozzle temperature of 210 °C. The volume fraction of fiber was about 12.5%. Fig. 2c presents the specimens with different geometric configurations manufactured by 3D printing.

2.3. Three-point bending tests

The quasi-static three-point bending tests were performed on a universal mechanical tester (Zwick Z050), and the fixed loading rate was determined to be 2 mm/min according to ASTM D7249/D7249M. The total length of all the specimens was 158 mm, and the span L between the supports was 110 mm. For each test, three specimens were measured to obtain the mean values of the bending properties. A digital camera was used to record the failure process of the specimens during the three-point bending.

2.4. Scanning electron microscope (SEM)

The local morphology of the 3D printed CFRCTCSs after bending failure was characterized by VEGA3 TESCAN scanning electron microscopy (SEM). Before the SEM analysis, the specimens were put into the ETD-800 small ion sputtering instrument for gold plating to improve the image quality.
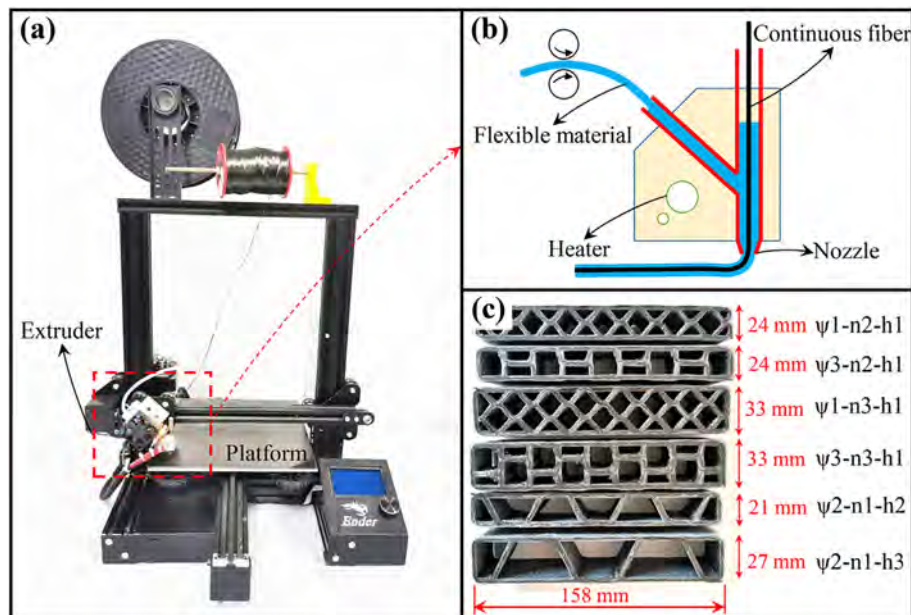

Fig. 2. Schematic diagram of 3D printing for integrated CFRCTCSs: (a) 3D printing equipment, (b) the scheme of the printing process and (c) the prepared CFRCTCSs with different geometric configurations.

2.5. Tests on the constituent material

Hou et al. [32] systematically investigated the tensile and compressive properties of 3D printed unidirectional continuous fiber reinforced PLA composite with various fiber volume fractions. When the fiber content is 12.5%, the longitudinal tensile strength and modulus are respectively 203.7 MPa and 17.0GPa, which are much higher than the compressive strength and modulus. This indicates that the first bending failure of the 3D printed CFRCTCSs will be mainly caused by the compression failure of the material. Therefore, according to the experimental method proposed by Du et al. [2], uniaxial compression tests were carried out on the 3D printed rectangular composite specimens to determine the mechanical properties of the constituent material. Four flat aluminum alloy blocks were fixed at both ends of the rectangular specimen to keep it vertical during the compression test, as shown in Fig. 3a. The effective length of the rectangular specimens was 16 mm. Fig. 3b and Fig. 3c present the typical failure mode and stress–strain curves of the specimens during compression, respectively. The average compressive modulus E of the constituent material is 3 GPa, and the compressive strength σ_c is 72.6 MPa.

2.6. Shape recovery tests

As shown in Fig. 4, there are three types of specimens used in the shape recovery tests, numbered ψ1-n3-h1, ψ2-n3-h1 and ψ3-n3-h1. The initial shape of all specimens is a rectangle with a geometric size of 158 × 33 × 1.2 mm. Under the temperature condition of 70 °C, the specimens were programmed into circular arc-shaped temporary shapes with an inner diameter of 32 mm. The shape recovery tests were conducted in a hot water bath at 60 °C. A digital camera was utilized to record the shape recovery process.

3. Theoretical investigation of bending behavior

3.1. Bending deflection

For a multi-layer corrugated sandwich beam loaded by three-point bending, the total deflection δ_F at its midpoint can be expressed as the sum of the deflections due to panel bending and core shearing [33]:

$$\delta_F = \frac{FL^3}{48(EI)_{eq}} + \frac{FL}{4(GA)_{eq}} \tag{2}$$

Where $(EI)_{eq}$ and $(GA)_{eq}$ are the equivalent bending stiffness and equivalent shear stiffness of the multilayer corrugated sandwich beam, respectively, which can be expressed as

$$(EI)_{eq} = \frac{Ebt_f^3}{6} + \frac{Ebt_f\left(h_c + t_f\right)^2}{2} + \frac{\bar{E}_x b h_c^3}{12} \tag{3}$$

$$(GA)_{eq} = \frac{b\left(h_c + t_f\right)^2}{h_c}\bar{G}_{xz} \tag{4}$$

Where, $\bar{E}_x$ is the in-plane equivalent elastic modulus of the corrugated core in the x-direction, and $\bar{G}_{xz}$ is the out-of-plane equivalent shear modulus of the corrugated core in the x-z plane. The detailed derivation of $\bar{E}_x$ and $\bar{G}_{xz}$ is given in Supplementary material section S2.1.
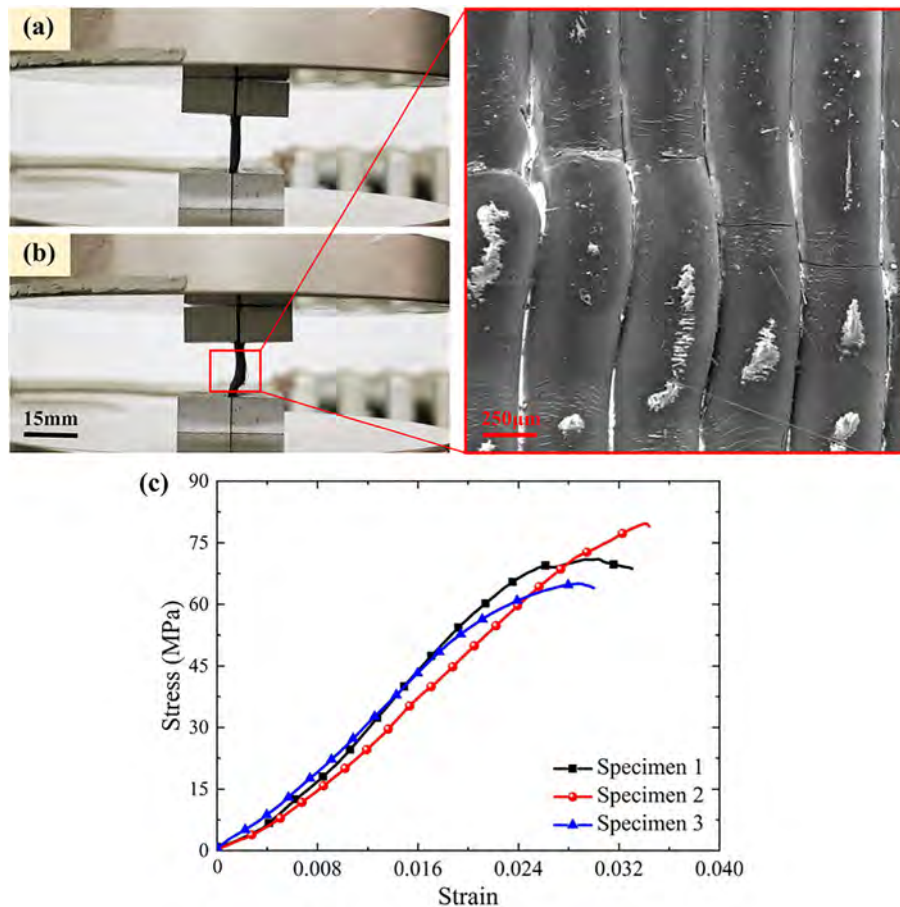

Fig. 3. Compression test of 3D printed continuous fiber reinforced composite: (a) specimen, (b) compressive failure mode and (c) measured stress–strain curves.
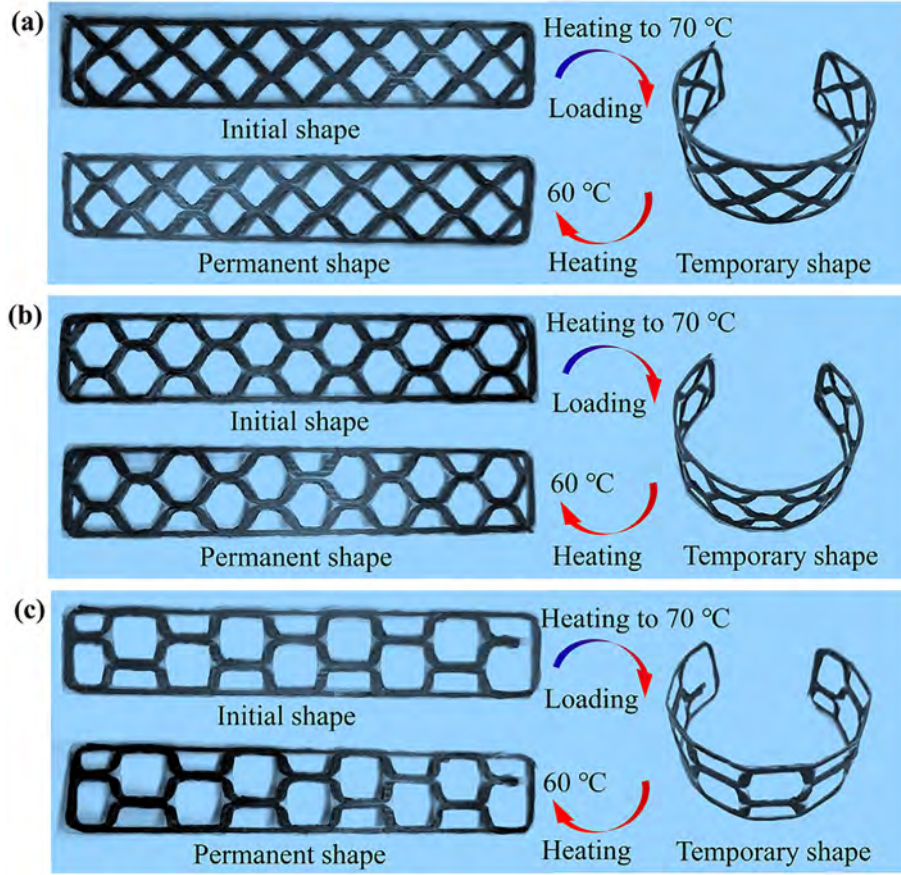
Fig. 4. The initial shapes, temporary shapes and permanent shapes of the 3D printed CFRCTCSs: (a) ψ1-n3-h1; (b) ψ2-n3-h1; (c) ψ3-n3-h1.

3.2. Bending failure load

The following failure modes may occur when a carbon fiber composite sandwich beam is subjected to three-point bending: 1) face yielding; 2) face buckling; 3) core shear failure; 4) indentation failure. The definitions of these bending failure modes are presented in Supplementary material section S1. The failure of a corrugated sandwich beam is usually determined by one of these competitive mechanisms, which depends on the geometry of the sandwich beam and the mechanical properties of the constituent material.

3.2.1. Face yielding

The face yielding occurs when the maximum normal stress in the panel reaches the yield stress of the constituent material. The constituent material is assumed to be completely elastoplastic. It represents face yielding only when the panel is completely plastically deformed. When the maximum stress occurs at the position of the maximum moment, which is the center of the beam, there is a balance equation [34]:

$$2b\left[\int_0^{h_c/2} \bar{E}_x \eta z^2 dz + \int_{h_c/2}^{h_c/2+t_f} \sigma_{fy} z dz\right] = \frac{FL}{4} \quad (5)$$

where, $\eta = \frac{2\sigma_{fy}}{h_c E}$ is a constant describing the distribution of equivalent strain along the cross-section of the beam.

Then, the critical load corresponding to the face yielding (FY) failure mode is

$$F_{fy} = \frac{12t_f(h_c + t_f) + 2h_c^2 \bar{E}}{3L} b\sigma_{fy} \quad (6)$$

Where, $\bar{E} = \bar{E}_x/E$.

3.2.2. Face buckling

The mutual coupling effect between the core and the panels is not considered in the analysis models. Under the lateral loading condition, the structural length of the panel corresponding to the trapezoidal core unit in the x-direction is small. Therefore, the face member is considered as a beam rigidly connected at both ends. The face beam length is $l_f = l + 2h c \cot\psi$, so the critical Euler buckling stress in the panel member can be expressed as [33]

$$\sigma_{fb} = \frac{\pi^2 E t_f^2}{3(l + 2hc\cot\psi)^2} \quad (7)$$

The critical load of face buckling (FB) failure mode can be obtained by replacing σ_{fy} with σ_{fb} in Eq. (6):

$$F_{fb} = \frac{\pi^2 b t_f^2 \left[12t_f(h_c + t_f)E + 2h_c^2 \bar{E}_x\right]}{9L(l + 2hc\cot\psi)^2} \quad (8)$$

3.2.3. Core shear failure

Under simply support conditions, the transverse shear force acting on the multi-layer sandwich beam by three-point bending is mainly borne by the corrugated core. The possible shear failure modes of the corrugated core are core member buckling (CB) and yielding (CY). Based on Eq. (S13) and Eq. (S14) in Supplementary material, expressions for estimating the critical load for the shear failure of the corrugated core can be obtained.

$$F_{cb} = \frac{4\pi^2 t^4 b h_c E \sin^3\psi}{3h^2(h\cos\psi + l\sin\psi)\left[(3h + t\cos\psi) + (3\lambda - t\sin\psi)C^F - 6C^M\right]} \quad (9)$$

$$F_{cy} = \frac{4t^2 b h_c \sin\psi \sigma_c}{(h\cos\psi + l\sin\psi)\left[(3h + t\cos\psi) + (3\lambda - t\sin\psi)C^F - 6C^M\right]} \quad (10)$$

where σ_c denotes the axial yield strength of the constituent material.

3.2.4. Indentation failure

The indentation collapse of the sandwich beam originates from the local elastic instability of the panel, accompanied by the local compression yielding of the core. The analysis model proposed by Craig A et al. [35] is utilized to predict the collapse failure load of a multi-layer periodic corrugated sandwich beam, in which the core is considered to be infinitely rigid-plastic. It is simply assumed that the core is subjected to a positive compressive force corresponding to the magnitude of the yield stress on the recessed portion of the panel. The maximum failure load is given as follows [35]

$$F_{\max} = bt_f \left[\frac{\pi^2 (h_c + t_f) E\sigma_c^2}{3L} \right]^{1/3} \tag{11}$$

Corresponding to the two different compression failure modes of the corrugated core, the failure load of the two indentation failure modes including the indentation failure induced by core web buckling (IB) and the indentation failure induced by core web yielding (IY) can be obtained from Eq. (S17) and Eq. (S18) in Supplementary material, respectively:

$$F_{ib} = bt_f \left[\frac{\pi^2 (h_c + t_f) E\sigma_{cb}^2}{3L} \right]^{1/3} \tag{12}$$

$$F_{iy} = bt_f \left[\frac{\pi^2 (h_c + t_f) E\sigma_{cy}^2}{3L} \right]^{1/3} \tag{13}$$

4. Results and discussion

4.1. Failure behavior

4.1.1. The effect of the number of core layers

To investigate the influence of the number of corrugated core layers on the bending performance and failure modes of the 3D printed CFRCTCSs, three kinds of sandwich structures with various numbers of layers (ie n1 = 1, n2 = 2 and n3 = 3) were investigated through three-point bending tests. These sandwich structures had the same corrugation angle ψ2 = 63° and the same single-layer core height h1 = 9 mm. Fig. 5 presents the load–displacement curves. It can be found that although these curves have different ultimate loads, they still exhibit similar evolutionary patterns. Specifically, the load increases almost linearly within a limited displacement range at the beginning. After the initial failure, the load peaks and then decreases with a considerable period of stable deformation. The peak loads of ψ2-n1-h1, ψ2-n2-h1 and ψ2-n3-h1 are 3.19 kN, 5.85 kN and 6.87 kN, respectively. It is obvious that the peak load increases with the number of layers *n*. The theoretical analysis had been performed to predict the critical failure loads of the 3D printed CFRCTCSs with different geometric parameters. The analytical predictions were compared with experimental results to verify the effectiveness of the proposed analysis models for predicting the bending properties and failure modes of the 3D printed CFRCTCSs. The dotted line in Fig. 5 represents the analytical prediction of the initial bending failure load for the corresponding specimen. The predicted values of the three specimens are 3.02 kN, 5.22 kN and 6.55 kN, respectively, which are 5.3%, 10.7% and 4.7% smaller than the experimental values, indicating that the analytical predictions are in good agreement with the experimental ones.

Fig. 6 records the photographs of the bending failure states of the 3D printed CFRCTCSs with the various number of core layers at two different moments. Corresponding to Fig. 6, Fig. 7 shows the local microscopic morphology of the failed specimens. State I corresponds
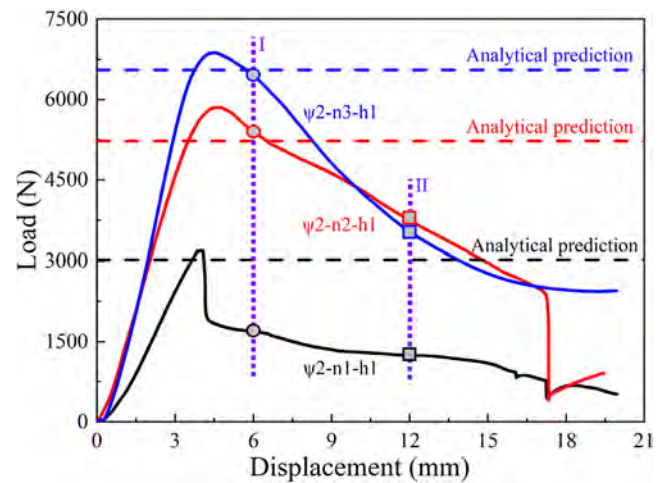

Fig. 5. Bending load–displacement responses of the 3D printed CFRCTCSs with the various number of corrugated core layers.

to the moment at which the circle symbols in Fig. 5 are located, and state II corresponds to the moment at which the rectangle symbols in Fig. 5 are located. From Fig. 6a and Fig. 7a, the face yielding failure of the specimen ψ2-n1-h1 during bending loading can be observed, which is consistent with the analytical prediction of the failure mode. This face yielding is attributed to the strong core configuration and the thin panels. Besides, the delamination and fracture of the inclined web of the trapezoidal corrugated core are also included during the bending process of the specimen ψ2-n1-h1.

Different from ψ2-n1-h1, the collapse mode of the 3D printed CFRCTCSs is dominated by the core shear failure when the number of layers is two. As shown in Fig. 6b, the initial failure mode of the specimen ψ2-n2-h1 is the matrix failure of the ends of the inclined member. It can be observed from Fig. 7b that obvious fibers pull-out and buckling occurred after the matrix failure, followed by matrix cracking and crack propagation. When the number of corrugated core layers is further increased from two to three, the increase of the initial failure load is significantly reduced, which is 61.7% less than the increase from one to two layers. The core shear collapse in the specimen ψ2-n3-h1 is observed in Fig. 6c and Fig. 7c. This collapse is caused by the shear fracture of the core member induced by the indentation failure of the beam.

4.1.2. The effect of corrugation angle

The effect of the corrugation angle on the bending performance of the 3D printed CFRCTCSs was evaluated by testing three types of sandwich beams with different corrugation angles (ie ψ1 = 52°, ψ2 = 63° and ψ3 = 90°). These sandwich structures had the same number of core layers n = 2 and the same single-layer core height h = 9 mm. The load–displacement curves corresponding to ψ1 = 52° and ψ3 = 90° are shown in Fig. 8. By combining Fig. 5 with Fig. 8, it can be known that the experimental peak load of ψ1-n2-h1, ψ2-n2-h1 and ψ3-n2-h1 are 6.12 kN, 5.85 kN and 3.74 kN, respectively. By applying the analysis models proposed in this paper, the predictions of the initial failure load for three sandwich specimens with various corrugation angles are 5.22 kN, 5.22 kN and 3.28 kN, which are 14.7%, 10.7% and 12.3% smaller than the experimental ones.

Fig. 9 demonstrates the impact of the corrugation angle on bending deformation and failure modes of the 3D printed CFRCTCSs. From Fig. 9a, it can be observed that the initial failure modes of ψ1-n2-h1 are mainly manifested as core shear failure caused by core member yielding. The plastic hinges appear at the joint between the upper panel and the core members. Moreover, the microscopic images in Fig. 10a show the matrix failure caused by fiber buckling at the joint
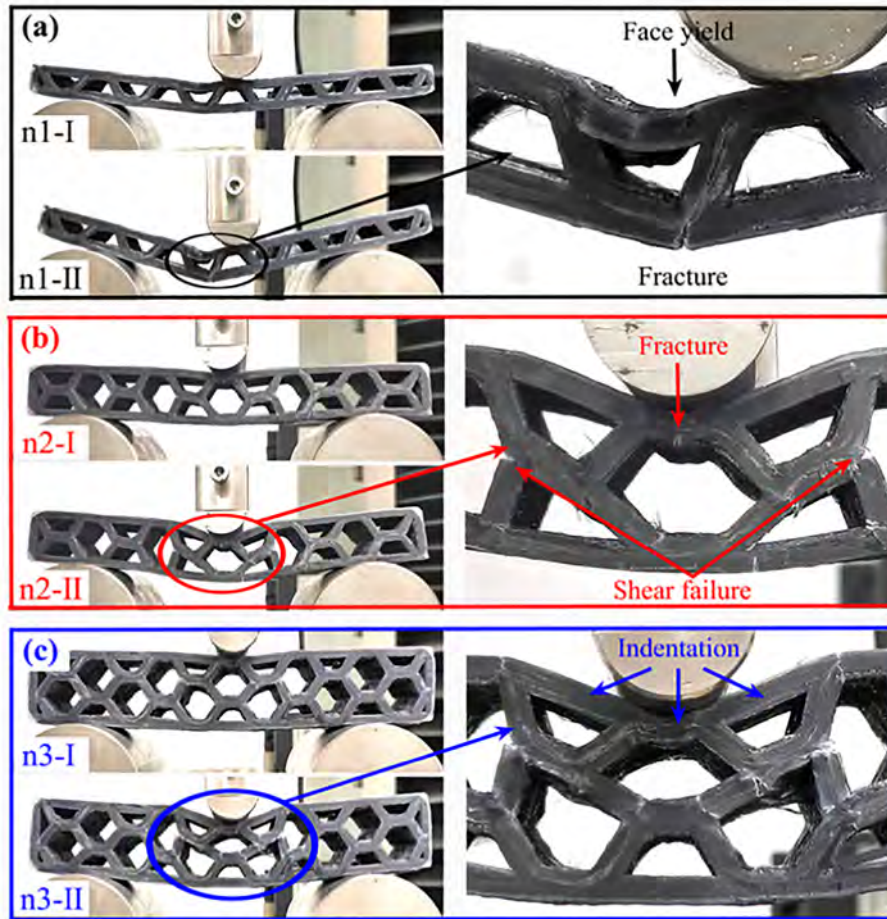
Fig. 6. Deformation processes and failure photographs of the 3D printed CFRCTCSs with different number of corrugated core layers: (a) ψ2-n1-h1; (b) ψ2-n2-h1; (c) ψ2-n3-h1.

of two corrugated cores. It can be found in Fig. 9b and Fig. 10b that the collapse of ψ3-n2-h1 is mainly caused by the shear yielding failure of the vertical core web. Matrix cracking and crack propagation occur at the nodes and eventually lead to fracture. This is consistent with the failure mode obtained by applying the proposed prediction models.

4.1.3. The effect of height of single-core

The single-layer sandwich structures with three different core heights (ie h1 = 9 mm, h2 = 15 mm and h3 = 21 mm) were considered in the three-point bending experiments. These single-layer sandwich structures had the same corrugation angle ψ = 63°. The load–displacement curves of the samples corresponding to h = 15 mm and h = 21 mm are plotted in Fig. 11, while the bending response of the samples corresponding to h = 9 mm is presented in Fig. 5. From Fig. 5 and Fig. 11, it can be determined that the experimental peak loads of ψ2-n1-h1, ψ2-n1-h2 and ψ2-n1-h3 are 3.19 kN, 2.16 kN and 1.53 kN, respectively. Obviously, the peak load is sensitive to changes in the height of the corrugated core because the second moment of inertia of the sandwich beam is affected by the height of the corrugated core. As the height of the corrugated core increases, inclined webs in the corrugated core withstand greater bending moments at the same load level, resulting in lower shear strength.

Bending deformation and collapse photographs of the 3D printed CFRCTCSs with different single-layer core heights are presented in Fig. 12. It can be observed from Fig. 12a that the breakage of the upper panel of ψ2-n1-h2 occurs under the indentation pressure of the

bending test fixture and then the crack occurs due to slippage. Fig. 12b indicates that the shear failure of the inclined core webs is the dominant collapse mode of ψ2-n1-h3 under bending loading. Besides, ψ2-n1-h3 is subjected to Euler buckling of the upper panel during core shear failure.

4.2. Flexural modulus and strength

For composite sandwich structures, the flexural modulus and bending strength can be calculated as follows [36]:

$$E_f = \frac{L^3}{4bH^3} \frac{F}{\delta_F} \quad (14)$$

$$\sigma_f = \frac{3P_{\max}L}{2bH^2} \quad (15)$$

where L is the span in the three-point bending experiment, H is the total thickness of the sandwich structure, P_{max} is the maximum load, and F / δ_F is the slope of the initial linear segment of the displacement-load curve. In this work, Eq. (2) was utilized to get F / δ_F, and then it was introduced into Eq. (14) to obtain the predicted value of the flexural modulus of various sandwich structures. The predicted value of bending strength was obtained based on the analytical value of the bending failure load. The comparison of the predictions and measurements of specific flexural modulus E_f / ρ_s and specific bending strength σ_f / ρ_s of the 3D printed CFRCTCSs with various geometric configurations is presented in Fig. 13.

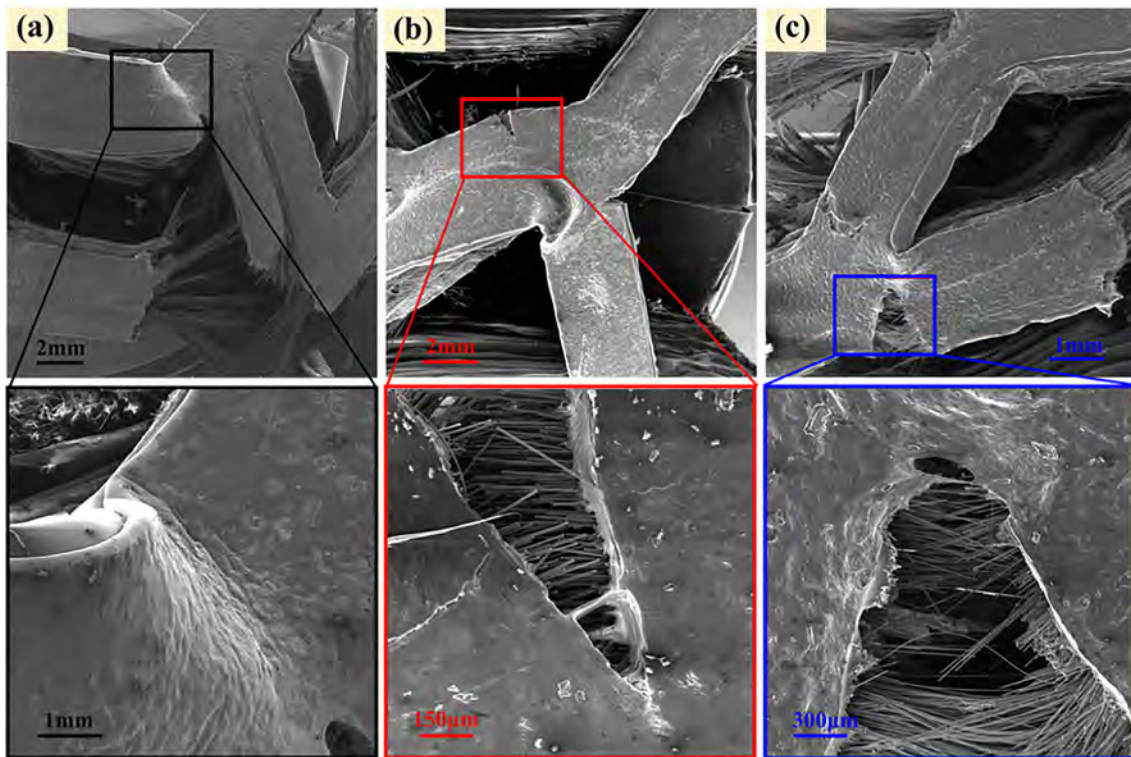**Fig. 7.** The local micromorphology of the 3D printed CFRCTCSs with different number of corrugated core layers: (a) ψ2-n1-h1; (b) ψ2-n2-h1; (c) ψ2-n3-h1.
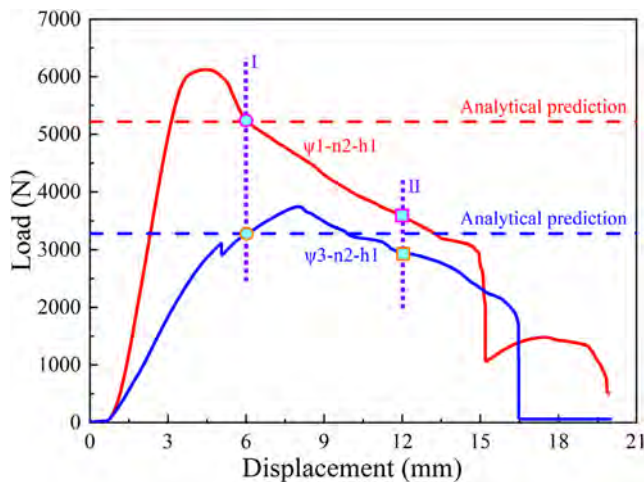

Fig. 8. The bending load–displacement responses of the 3D printed CFRCTCSs with various corrugation angles.

It can be seen from Fig. 13a that whether the experimental value or the predicted value, the E_f / ρ_s gradually decreases as the number of corrugated core layers n increases. This proves that the single-layer sandwich structure possesses a higher specific flexural modulus when other structural parameters are fixed. By comparing three sandwich structures of ψ1-n1-h1, ψ2-n1-h1 and ψ3-n1-h1 with the single-layer corrugated core, it is found that ψ1-n1-h1 and ψ2-n1-h1 have remarkably higher predicted and experimental values of the specific modulus. The same conclusion can be drawn by comparing the three sandwich structures of ψ1-n2-h1, ψ2-n2-h1 and ψ3-n2-h1 with double corrugated cores. It can be concluded that when the corrugation angle is 90°, CFRCTCSs have a lower specific flexural modulus, which may be due to the crushing failure that the vertical core webs tend to occur.

Besides, the single-layer core height makes a considerable impact on the flexural modulus of the 3D printed CFRCTCSs. The experimental values of the specific modulus of ψ2-n1-h1, ψ2-n1-h2 and ψ2-n1-h3 with single-layer core heights of 9 mm, 15 mm and 21 mm are 2.98×10^6 m²/s², 0.82×10^6 m²/s² and 0.38×10^6 m²/s², respectively. Obviously, as the single-layer core height increases, the specific flexural modulus of the sandwich structure decreases sharply. This is mainly because a larger single-layer core height means a longer core web, which is more vulnerable to shear yield failure, resulting in lower bending resistance of the structure.

Similar to E_f / ρ_s, it can be observed from Fig. 13b that the specific bending strength σ_f / ρ_s of CFRCTCSs decreases with an increase in the number of core layers n. Theoretical and experimental results are close but still exist a certain deviation, which may be caused by external disturbances during the measurements. It is worth noting that when the number of core layers is one, the specific strength of the specimen with a corrugation angle of 90° is not significantly lower than that of the specimen with a corrugation angle of 52° or 63°. This implies that although the corrugation angle of 90° reduces the flexural modulus of single-layer CFRCTCSs, it makes no adverse effect on the bending strength. By comparing the 3D printed CFRCTCSs with various corrugation angles but the same number of core layers, it can be concluded that setting the corrugation angle to 63° contributes to higher specific bending strength.

4.3. Failure mechanism maps

Failure maps are important for designing corrugated sandwich structures with several potential failure modes. In this section, the proposed analysis models were used to construct the failure maps which could reveal the dominant initial failure mechanism of the 3D printed CFRCTCSs. As shown in Fig. 14, with the dimensionless parameters t_f / L and h / L as the abscissa and ordinate, respectively, the initial failure mode maps of the 3D printed CFRCTCSs with single-layer corrugated core under three-point bending were
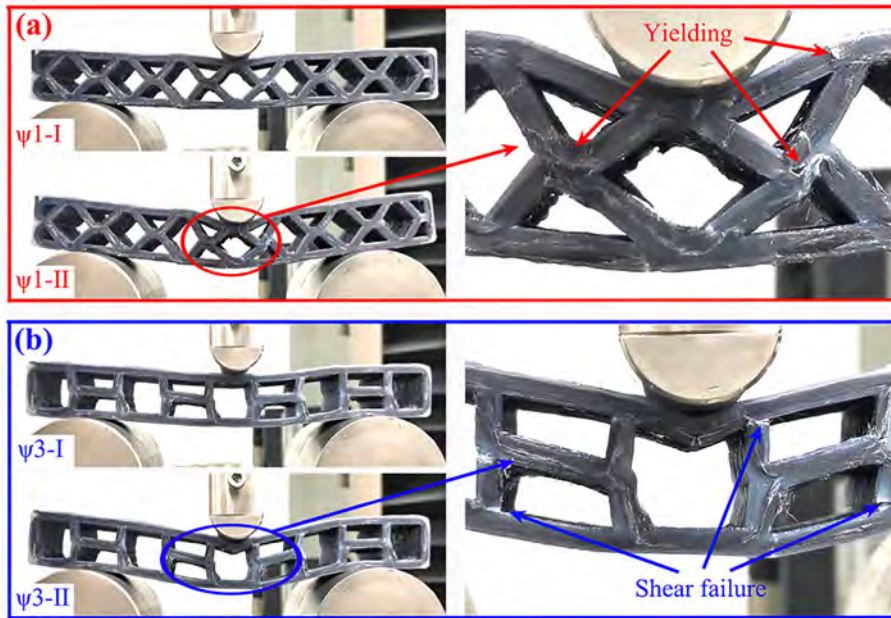
Fig. 9. Bending deformation and failure modes of the 3D printed CFRCTCSs with various corrugation angles: (a) ψ1-n2-h1; (b) ψ3-n2-h1.
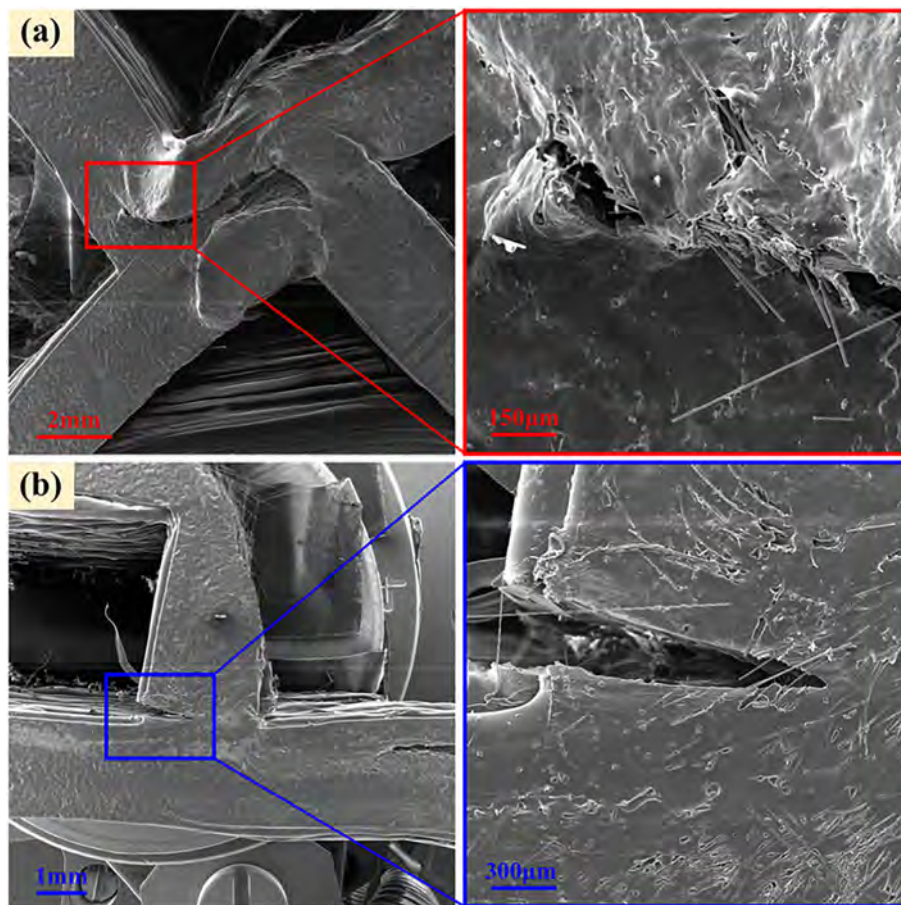

Fig. 10. The local micromorphology of the 3D printed CFRCTCSs with various corrugation angles: (a) ψ1-n2-h1; (b) ψ3-n2-h1.

constructed by Eq. (6), Eq. (8), Eq. (9) and Eq. (10) considering three kinds of corrugation angles. The material properties and other geometric parameters were constant.

The failure mechanism map corresponding to each specific corrugation angle can be divided into four regions, and in each region a specific failure mechanism is dominant. Obviously, the transition line
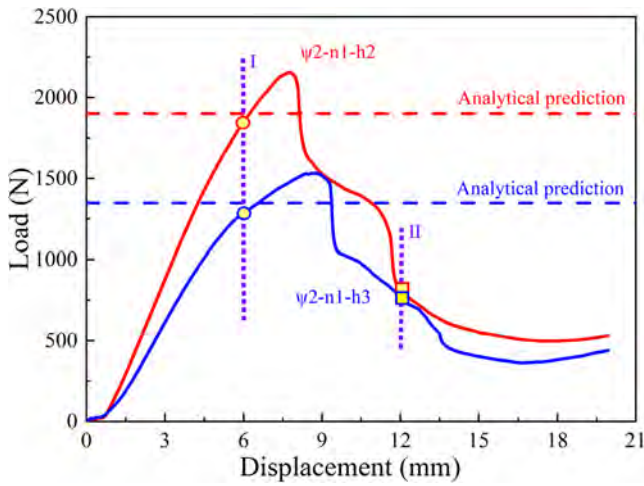
Fig. 11. Bending load–displacement curves of the 3D printed CFRCTCSs with the various heights of single-core.
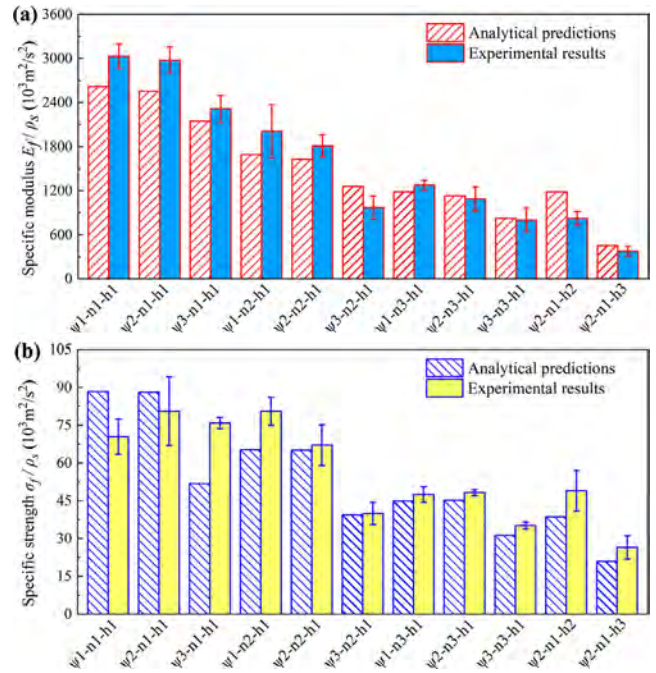

Fig. 13. Comparison of analytical predictions and experimental results of specific bending properties for the 3D printed CFRCTCSs: (a) Specific flexural modulus E_f / ρ_s; (b) Specific bending strength σ_f / ρ_s.

between any two failure modes mainly depends on the strength and geometric parameters of the panels and corrugated core. In the case of high t_f / L and h / L, the core shear failure induced by Euler buckling of the inclined core webs is the main collapse mechanism due to the strong panels and long inclined core webs. In the case of low t_f / L, the face failure caused by Euler buckling is the primary failure mode due to the thin panels. Fig. 14 also presents the influence of the corrugation angle ψ on the transition line between various failure mechanisms. As the corrugation angle increases, the incidence of core shear failure caused by the inclined web yielding increases, while the incidence for the other three failure mechanisms including face yielding, face buckling and core buckling is reduced.

Fig. 15 illustrates the prediction maps of the initial failure for the 3D printed CFRCTCSs with specific single-layer core height. The experimental data is added to the maps with different symbols representing the corresponding failure modes. Fig. 15a depicts that the competitive failure modes for $h = 9$ mm are face yielding (FY), core member yielding (CY) and indentation failure induced by core web yielding (IY). Near the transition line between face yielding and indentation failure modes, experimental results and analytical predictions are inconsis-

tent. This is mainly caused by experimental errors and mixed failure modes. Except for the vicinity of the transition lines, the predictions in other areas are consistent with the experimental results.

Fig. 15b shows the failure mechanism diagram for the 3D printed CFRCTCSs with $h = 15$ mm. Compared with the corresponding value of $h = 9$ mm, the map is shifted slightly to the left and the area of core shear yielding is expanded. All experimental observations are located in the area of core shear yielding, which agrees with the analytical prediction. Besides, with lower H / L and ψ, the dominant failure mode is converted from face yielding to face buckling. Different from the failure mechanism map corresponding to $h = 15$ mm, the initial failure map corresponding to $h = 21$ mm is dominated by five failure modes,
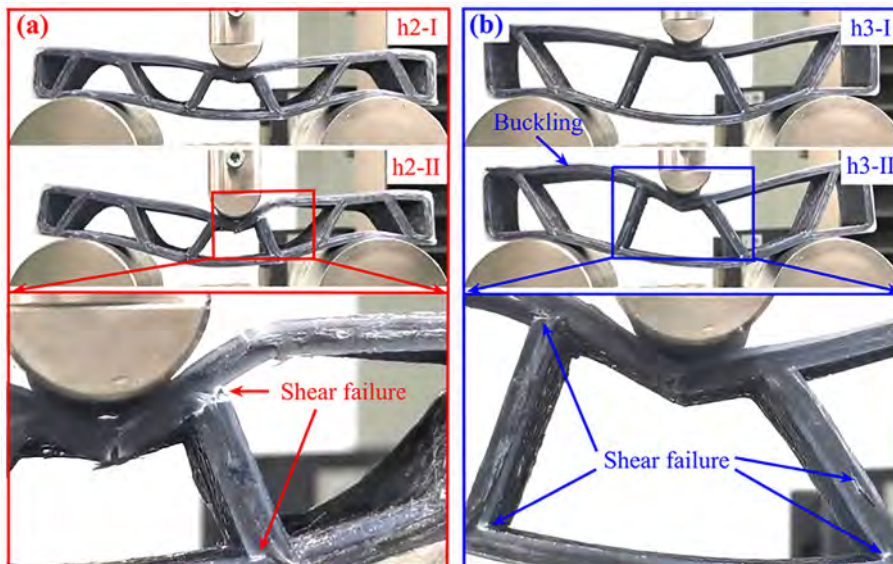

Fig. 12. Bending deformation and collapse modes of the 3D printed CFRCTCSs with the various heights of single-core: (a) $h = 15$ mm; (b) $h = 21$ mm.
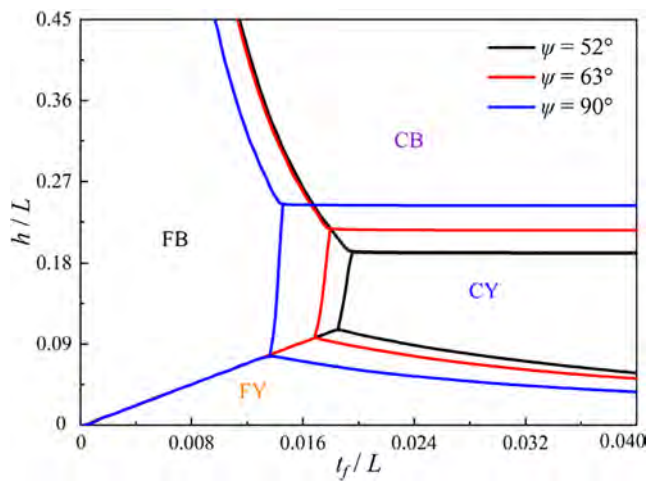
Fig. 16. Demonstrations of the shape recovery process of the 3D printed CFRCTCS numbered ψ3-n3-h1 at 60 ℃.

Fig. 17. (a) Flexural modulus and (b) bending strength versus density maps for the 3D printed CFRCTCSs compared to other competing sandwich structures.

5. Comparison of competing structures

The material property charts provide a convenient way to compare the mechanical properties of the 3D printed CFRCTCSs with sandwich structures which are fabricated by various methods. Fig. 17a an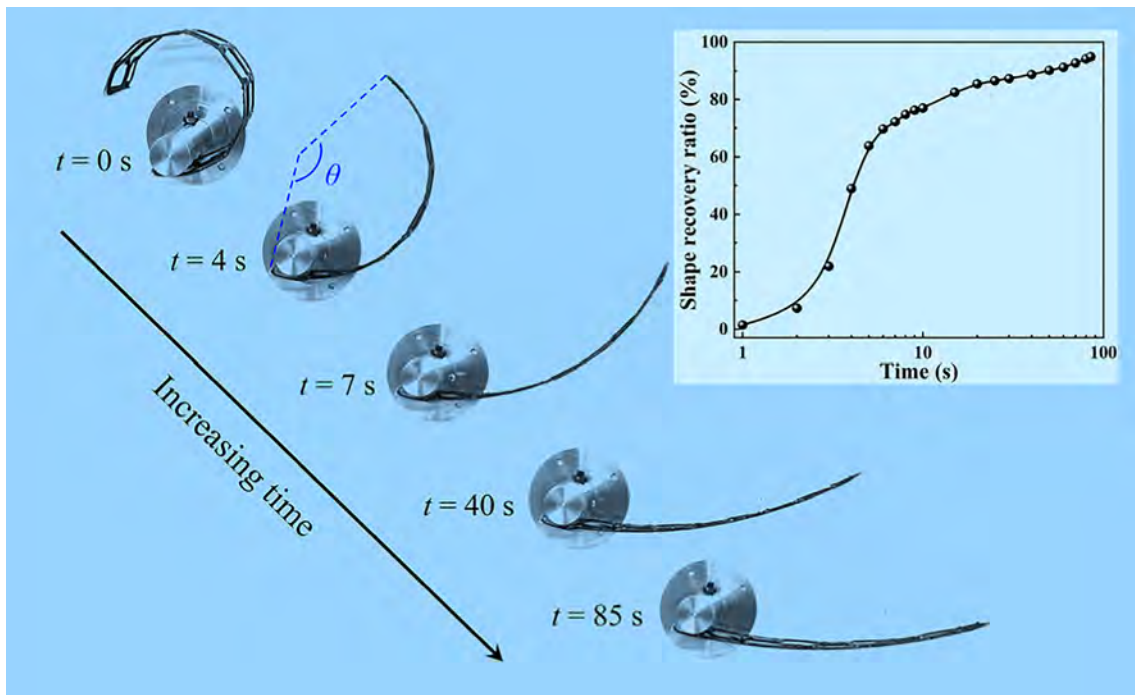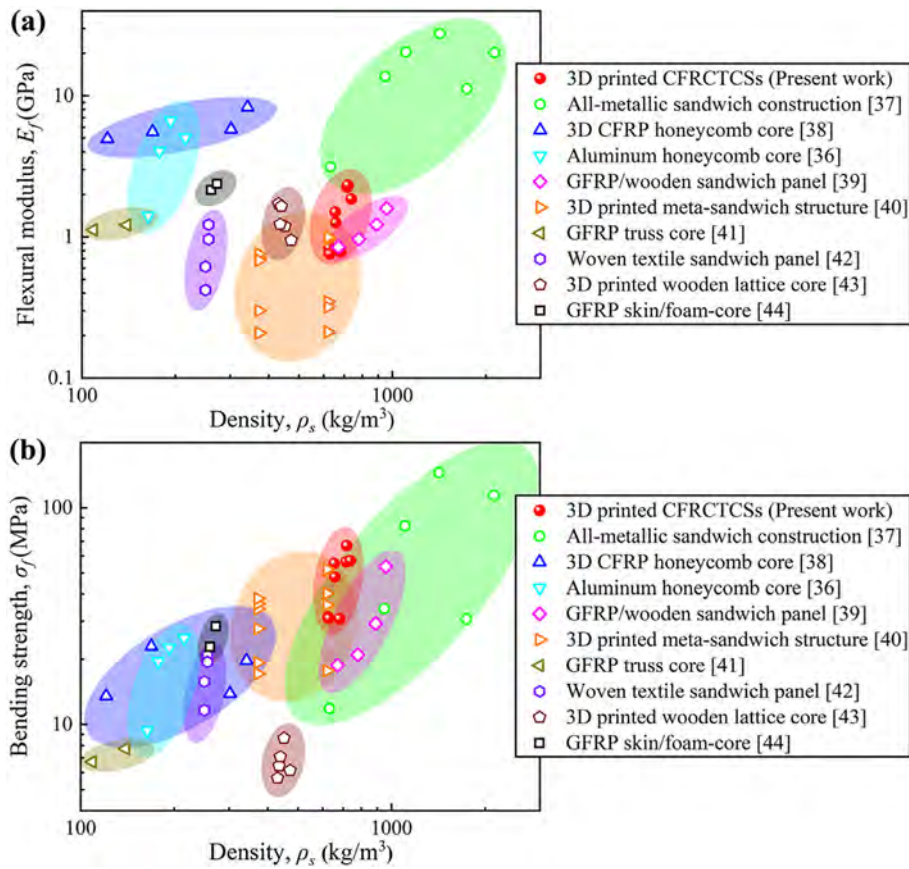d 17b compare separately the measured bending modulus E_f and bending strength σ_f of the 3D printed CFRCTCSs with several competitive sandwich structures, including all-metallic hybrid-cored sandwich constructions [37], 3D CFRP honeycomb sandwich beams [38], CFRP skin/aluminum honeycomb core sandwich structures [36], GFRP/wooden sandwich panels [39], 3D printed *meta*-sandwich structures [40], GFRP truss core panels [41], woven textile sandwich panels [42], 3D printed lattice core sandwich beams [43] and GFRP skin/foam core sandwich structures [44].

The results in Fig. 17 demonstrates that the 3D printed CFRCTCSs possess higher flexural modulus and bending strength than conventional 3D printed sandwich structures such as polymer *meta*-sandwich structures [40]. This proves that the 3D printing method of the continuous fiber reinforced polymer composite sandwich structure involved in this work has considerable advantages and potential compared to the general single-material 3D printing process. It is noted that the bending resistance of the 3D printed CFRCTCSs is considerably more competitive than GFRP / wooden sandwich panels [39] and woven textile sandwich panels [42] manufactured by hot-press molding methods, and comparable with CFRP skin/aluminum honeycomb core sandwich structures [36]. Additionally, Fig. 17a suggests that the flexural modulus of all-metallic hybrid-cored sandwich constructions [37] and CFRP sandwich beams with egg or pyramidal honeycomb cores [38] is superior to the remaining sandwich structures including the 3D printed CFRCTCSs described herein. However, Fig. 17b confirms the stronger bending strength of the 3D printed CFRCTCSs than other sandwich structures, which exhibits the broad application prospects of the 3D printed CFRCTCSs in high-strength and lightweight structures.

6. Conclusion

In this paper, CFRCTCSs were fabricated by combining SMPs and FFF-based 3D printing process and were experimentally investigated under three-point bending. The initial failure load, flexural modulus and bending strength of the 3D printed CFRCTCSs were predicted through theoretical analysis. The failure mechanism maps based on the proposed analysis models were constructed to predict the failure modes of CFRCTCSs. The analytical predictions match well with experimental measurements. Besides, the shape memory capability of the 3D printed CFRCTCSs was characterized by shape recovery tests. Based on the results and discussion in this article, the following conclusions can be drawn:

1) Increasing the number of core layers improves the peak failure load of the 3D printed CFRCTCSs but leads to lower specific flexural modulus and specific bending strength.
2) There is little difference in the bending performance of the 3D printed CFRCTCSs when the corrugation angle is 52° or 63°, while CFRCTCSs with a corrugation angle of 90° have obviously lower specific modulus due to the vertical core webs are prone to shear failure.
3) The increase in core height causes the initial failure mode of the 3D printed CFRCTCSs to change from face yielding to core member yielding and core buckling due to Euler buckling of the slender core web, during which the specific properties of the structure are dramatically reduced.
4) The 3D printed CFRCTCSs possesses excellent shape memory performance, and the maximum shape recovery ratio is as high as 95%.

5) Comparison with several competitive sandwich structures demonstrates that the 3D printed CFRCTCSs have outstanding bending properties.

CRediT authorship contribution statement

Chengjun Zeng: Conceptualization, Investigation, Visualization, Validation, Writing - original draft, Writing - review & editing. **Liwu Liu:** Methodology, Formal analysis, Data curation, Validation, Writing - review & editing. **Wenfeng Bian:** Investigation, Visualization, Writing - review & editing. **Jinsong Leng:** Investigation, Validation, Writing - review & editing. **Yanju Liu:** Conceptualization, Investigation, Supervision, Writing - review & editing.

Declaration of Competing Interest

The authors declare that they have no known competing financial interests or personal relationships that could have appeared to influence the work reported in this paper.

Acknowledgements

Appendix A. Supplementary data

Supplementary data to this article can be found online at https://doi.org/10.1016/j.compstruct.2021.113626.

References

[1] Atashipour SR, Al-Emrani M. A realistic model for transverse shear stiffness prediction of composite corrugated-core sandwich elements. Int J Solids Struct 2017;129:1–17.
[2] Du Y, Song C, Xiong J, Wu L. Fabrication and mechanical behaviors of carbon fiber reinforced composite foldcore based on curved-crease origami. Compos Sci Technol 2019;174:94–105.
[3] Zhang F, Liu W, Fang H, Jia Z. Flexural behavior of composite sandwich beams with different kinds of GFRP ribs in flatwise and edgewise positions. Compos Part B: Eng 2019;156:229–39.
[4] Shaban M, Alibeigloo A. Three-dimensional elasticity solution for sandwich panels with corrugated cores by using energy method. Thin Wall Struct 2017;119:404–11.
[5] Mesquita F, van Gysel A, Selezneva M, Swolfs Y, Lomov SV, Gorbatikh L. Flexural behaviour of corrugated panels of self-reinforced polypropylene hybridised with carbon fibre: An experimental and modelling study. Compos Part B: Eng 2018;153:437–44.
[6] Rejab MRM, Cantwell WJ. The mechanical behaviour of corrugated-core sandwich panels. Compos Part B: Eng 2013;47:267–77.
[7] Dayyani I, Shaw AD, Saavedra Flores EI, Friswell MI. The mechanics of composite corrugated structures: A review with applications in morphing aircraft. Compos Struct 2015;133:358–80.
[8] Seong DY, Jung CG, Yang DY, Moon KJ, Ahn DG. Quasi-isotropic bending responses of metallic sandwich plates with bi-directionally corrugated cores. Mater Des 2010;31:2804–12.
[9] Valdevit L, Wei Z, Mercer C, Zok FW, Evans AG. Structural performance of near-optimal sandwich panels with corrugated cores. Int J Solids Struct 2006;43:4888–905.
[10] Hu Y, Li W, An X, Fan H. Fabrication and mechanical behaviors of corrugated lattice truss composite sandwich panels. Compos Sci Technol 2016;125:114–22.
[11] Schneider C, Kazemahvazi S, Zenkert D, Deshpande VS. Dynamic compression response of self-reinforced poly (ethylene terephthalate) composites and corrugated sandwich cores. Compos Part A: Appl Sci Manuf 2015;77:96–105.
[12] Chacón JM, Caminero MA, Núñez PJ, García-Plaza E, García-Moreno I, Reverte JM. Additive manufacturing of continuous fibre reinforced thermoplastic composites using fused deposition modelling: Effect of process parameters on mechanical properties. Compos Sci Technol 2019;181:107688.
[13] Quadrini F, Squeo EA. Injection molding of bushes made of tribological PEEK composites. Express Polym Lett 2007;1:817–23.
[14] Zhao W, Zhang F, Leng J, Liu Y. Personalized 4D printing of bioinspired tracheal scaffold concept based on magnetic stimulated shape memory composites. Compos Sci Technol 2019;184:107866.
[15] Liu T, Liu L, Zeng C, Liu Y, Leng J. 4D printed anisotropic structures with tailored mechanical behaviors and shape memory effects. Compos Sci Technol 2020;186:107935.

[16] Wei H, Cauchy X, Navas IO, Abderrafai Y, Chizari K, Sundararaj U, et al. Direct 3D Printing of Hybrid Nanofiber-Based Nanocomposites for Highly Conductive and Shape Memory Applications. ACS Appl Mater Interfaces 2019;11:24523–32.

[17] Tan WS, Chua CK, Chong TH, Fane AG, Jia A. 3D printing by selective laser sintering of polypropylene feed channel spacers for spiral wound membrane modules for the water industry. Virtual Phys Prototyp 2016;11:151–8.

[18] Kuang X, Roach DJ, Wu J, Hamel CM, Ding Z, Wang T, et al. Advances in 4D printing: Materials and applications. Adv Funct Mater 2019;29:1805290.

[19] Seyedkanani A, Niknan H, Akbarzadeh AH. Bending behavior of optimally graded 3D printed cellular beams. Addit Manuf 2020;35:101327.

[20] Li F, Liu L, Lan X, Zhou X, Bian W, Liu Y, et al. Preliminary design and analysis of a cubic deployable support structure based on shape memory polymer composite. Int J Smart Nano Mater 2016;7:106–18.

[21] Zhao W, Liu L, Leng J, Liu Y. Thermo-mechanical behavior prediction of particulate reinforced shape memory polymer composite. Compos Part B: Eng 2019;179:107455.

[22] Tao R, Xi L, Wu W, Li Y, Liao B, Liu L, et al. 4D Printed Multi-stable Metamaterials with Mechanically Tunable Performance. Compos Struct 2020;252:112663.

[23] Heidari-Rarani M, Rafiee-Afarani M, Zahedi AM. Mechanical characterization of FDM 3D printing of continuous carbon fiber reinforced PLA composites. Compos Part B: Eng 2019;175:107147.

[24] Luo M, Tian X, Shang J, Zhu W, Li D, Qin Y. Impregnation and interlayer bonding behaviours of 3D-printed continuous carbon-fiber-reinforced poly-ether-ether-ketone composites. Compos Part A: Appl Sci Manuf 2019;121:130–8.

[25] Caminero MA, Chacón JM, García-Moreno I, Rodríguez GP. Impact damage resistance of 3D printed continuous fibre reinforced thermoplastic composites using fused deposition modelling. Compos Part B: Eng 2018;148:93–103.

[26] Zeng C, Liu L, Bian W, Liu Y, Leng J. 4D printed electro-induced continuous carbon fiber reinforced shape memory polymer composites with excellent bending resistance. Compos Part B: Eng 2020;194:108034.

[27] Quan C, Han B, Hou Z, Zhang Q, Tian X, Lu T. 3d printed continuous fiber reinforced composite auxetic honeycomb structures. Compos Part B: Eng 2020;187:107858.

[28] Hou Z, Tian X, Zhang J, Li D. 3D printed continuous fibre reinforced composite corrugated structure. Compos Struct 2018;184:1005–10.

[29] Sugiyama K, Matsuzaki R, Ueda M, Todoroki A, Hirano Y. 3D printing of composite sandwich structures using continuous carbon fiber and fiber tension. Compos Part A: Appl Sci Manuf 2018;113:114–21.

[30] K. Essassi J.-l. Rebiere A. El Mahi M.A. Ben Souf A. Bouguecha M. Haddar Experimental and analytical investigation of the bending behaviour of 3D-printed bio-based sandwich structures composites with auxetic core under cyclic fatigue tests Compos Part A: Appl Sci Manuf 2020;131:105775.

[31] Zhang W, Zhang F, Lan X, Leng J, Wu AS, Bryson TM, et al. Shape memory behavior and recovery force of 4D printed textile functional composites. Compos Sci Technol 2018;160:224–30.

[32] Hou Z, Tian X, Zheng Z, Zhang J, Zhe L, Li D, et al. A constitutive model for 3D printed continuous fiber reinforced composite structures with variable fiber content. Compos Part B: Eng 2020;189:107893.

[33] Xu G, Wang Z, Zeng T, Cheng S, Fang D. Mechanical response of carbon/epoxy composite sandwich structures with three-dimensional corrugated cores. Compos Sci Technol 2018;156:296–304.

[34] Jiang B, Li Z, Lu F. Failure mechanism of sandwich beams subjected to three-point bending. Compos Struct 2015;133:739–45.

[35] Steeves CA, Fleck NA. Collapse mechanisms of sandwich beams with composite faces and a foam core, loaded in three-point bending. Part I: analytical models and minimum weight design. Int J Mech Sci 2004;46:561–83.

[36] Wang J, Shi C, Yang N, Sun H, Liu Y, Song B. Strength, stiffness, and panel peeling strength of carbon fiber-reinforced composite sandwich structures with aluminum honeycomb cores for vehicle body. Compos Struct 2018;184:1189–96.

[37] Yan L, Han B, Yu B, Chen C, Zhang Q, Lu T. Three-point bending of sandwich beams with aluminum foam-filled corrugated cores. Mater Des 2014;60:510–9.

[38] Xiong J, Ma L, Stocchi A, Yang J, Wu L, Pan S. Bending response of carbon fiber composite sandwich beams with three dimensional honeycomb cores. Compos Struct 2014;108:234–42.

[39] Hussain M, Abbas N, Zahra N, Sajjad U, Awan MB. Investigating the performance of GFRP/wood-based honeycomb sandwich panels for sustainable prefab building construction. SN Appl Sci 2019;1:875.

[40] Yazdani Sarvestani H, Akbarzadeh AH, Mirbolghasemi A, Hermenean K. 3D printed meta-sandwich structures: Failure mechanism, energy absorption and multi-hit capability. Mater Des 2018;160:179–93.

[41] Djama K, Michel L, Gabor A, Ferrier E. Mechanical behaviour of a sandwich panel composed of hybrid skins and novel glass fibre reinforced polymer truss core. Compos Struct 2019;215:35–48.

[42] Fan H, Zhou Q, Yang W, Zheng J. An experiment study on the failure mechanisms of woven textile sandwich panels under quasi-static loading. Compos Part B: Eng 2010;41:686–92.

[43] Smardzewski J, Wojciechowski KW. Response of wood-based sandwich beams with three-dimensional lattice core. Compos Struct 2019;216:340–9.

[44] Kaboglu C, Yu L, Mohagheghian I, Blackman BR, Kinloch AJ, Dear JP. Effects of the core density on the quasi-static flexural and ballistic performance of fibre-composite skin/foam-core sandwich structures. J Mater Sci 2018;53:16393–414.